Skin color modeling using the radiative transfer equation solved by the auxiliary function method

Caroline Magnain,* Mady Elias, and Jean-Marc Frigerio

Institut des NanoSciences de Paris, Campus Boucicaut, 140 rue de Lourmel, 75015 Paris, France
*Corresponding author: caroline.magnain@insp.jussieu.fr

The auxiliary function method is an efficient technique for solving the radiative tranfer equation without adding any assumption and was applied until now only for theoretical stratified media. The first application (to our knowledge) of the method to a real case, the human skin, is presented. This makes it possible to validate the method by comparing model results with experimental reflectance spectra of real skin. An excellent agreement is obtained for a multilayer model of the skin made of 22 sublayers and taking into account the anisotropic phase function of the scatterers. Thus there is the opportunity to develop interest in such models by quantitatively evaluating the influence of the parameters commonly used in the literature that modify skin color, such as the concentration of the scatterers and the thickness of each sublayer. © 2007 Optical Society of America

OCIS codes: 030.5620, 170.3660, 290.4210, 300.6550, 330.1690.

1. INTRODUCTION

Modeling skin color is of great interest, with diverse applications such as in cosmetics and in computer rendering. It needs a topographic model of the skin, which is a very complex structure [1] containing different layers (at least epidermis, dermis, and hypodermis) and several scatterers (melanosomes, blood cells, keratin, and collagen). The light propagation can then be described by using the radiative transfer equation [2] (RTE) that leads to reflectance spectra and trichromatic coordinates of human skin.

Several attempts to model skin appearance following this scheme have already been published, two of which are close to the process that is applied here. A rather similar study has been undertaken by Poirier [3] in the framework of skin color rendering in computer graphics. His modeling is based on a four-layer skin model and uses the Kubelka–Munk [4] two-flux method, which cannot take into account the size of the scatterers and especially the already known fragmentation [5] of the melanosomes in the epidermis. Its experimental validation is rather satisfactory in the middle of the visible range, but not for small and large wavelengths. The influence of different parameters on the reflectance spectra, such as the concentration of the various scatterers and the thickness of the different layers, is studied there; the results are interesting but cannot be compared with ours, since the values of the fixed parameters are not given. Another work carried out by Nielsen [6] presents skin modeling mostly in the UV domain. It takes into account the fragmentation of melanosomes as they move up in the epidermis. It uses the discrete-ordinate method [7] to solve the RTE. The model of the present work is inspired by Nielson's 7-layer model and has been developed into a 22-layer model. In our

work, the optical properties of the melanosomes are directly calculated from Mie theory [8] without using the simplified reduced scattering coefficients employed in the previous paper. Unlike asymptotic methods, the *N*-flux method [9] and the discrete-ordinate method [7], an exact method is used here, the auxiliary function method [10] (AFM). This method has already been successfully developed for monolayers to explain the visual aspect of art glazes [11]. The same method has also been developed for multilayers but has been applied only in theoretical cases [12]. The presented study deals with human Caucasian skin, which is a concrete case, and it will allow the model to be validated for the first time to our knowledge with experiments for multilayer media.

In Section 2, the RTE [2] is recalled and written for diffuse flux, and the general AFM [12] is summarized. Section 3 presents the structure of human Caucasian skin, the optical properties of the main scatterers, and the measured reflectance spectra of real skins. In Section 4, a final 22-layer model is presented, and the modeled and measured reflectance spectra are compared. For the first time to our knowledge the good agreement validates the efficient AFM with experiments on a real case. The interest of such modeling is then developed by quantitatively evaluating the influence of the parameters, commonly used in the literature, that modify skin color, such as the concentration of the scatterers, the oxygen saturation of blood, and the thickness of each sublayer, and finally the influence of the five parameters.

2. RTE AND AFM

The AFM has already been developed to solve the RTE in inhomogeneous stratified scattering media [12]. It has

been applied to theoretical systems with a continuously varying albedo and phase function, with different refractive index in sublayers. The present work deals with the application of AFM for the human skin, which is a real stratified medium. The results of simulations can be compared with measurements, which would not be possible for theoretical models. Although the RTE can be solved with the AFM for a stratified medium with a different refractive index in each layer by using Fresnel and Snell laws for boundary conditions at each interface, our application on skin will use only one refractive index in all layers. The Fresnel and Snell laws are then used only at both extreme interfaces. We present here only an overview of the RTE solved by the AFM applied to our system. All the details of the method can be found in a previous paper [12], and the same notation is used throughout.

We consider a medium containing scatterers, assumed to be spherical to allow us to simply use Mie theory [8]. These scatterers are in low concentration, and the incident light is incoherent and unpolarized so that the RTE can be applicable. Moreover, the incident light is collimated in the direction of a unit vector $\mathbf{u}_0$ outside the system defined by the angle θ_0 as shown in Fig. 1. The interfaces of this system are supposed to be planes. The collimated and diffuse flux, respectively, are denoted F and f. Figure 1 summarizes collimated flux and diffuse flux created by single (1) and multiple (2) scattering inside the medium. The purpose of the calculation is to express both reflected flux outgoing from the system for each wavelength and for all directions in order to obtain its reflectance spectrum, which is accessible to experiments.

The collimated flux F is calculated separately. It is refracted at the first air–medium interface, following Fresnel and Snell laws. F will then keep the same direction $\mathbf{u}'$ inside the system. In our case, the incident collimated light will be taken normal to the surface ($\theta_0 = 0°$) to match the experimental conditions.

The diffuse flux are calculated by using the RTE, which expresses the diffuse flux balance through an homogeneous elementary slab with an optical thickness $d\tau$. It is written for a given wavelength λ, depth z, and direction, defined by the angles θ and ϕ or by the unit vector $\mathbf{u}$. The scatterers embedded in the medium are characterized by their absorption and scattering coefficients, respectively, k and s. The albedo $\varpi = s/(k+s)$ and the optical depth $\tau = \int_0^z (k+s) dz$ are used as reduced quantities to write the RTE:
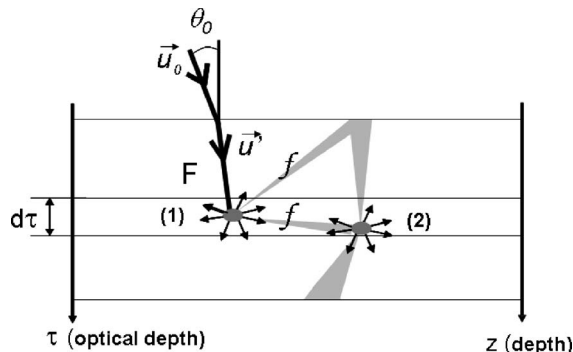

Fig. 1. Collimated flux and diffuse flux created by single and multiple scattering inside the medium.

$$\frac{df(\mathbf{u},\tau)}{d\tau} = -\frac{f(\mathbf{u},\tau)}{\mu} + \frac{\varpi}{4\pi}\frac{\mu}{|\mu|}\frac{F(\mathbf{u}',\tau)}{|\mu'|}p(\mathbf{u},\mathbf{u}')$$
$$+ \frac{\varpi}{4\pi}\frac{\mu}{|\mu|}\int_0^{4\pi}\frac{f(\mathbf{u}_1,\tau)}{|\mu_1|}p(\mathbf{u},\mathbf{u}_1)d\Omega_1, \quad (1)$$

where $\mu = \cos\theta$ and $p(\mathbf{u},\mathbf{u}_i)$ is the phase function describing the probability for an incident light with the direction $\mathbf{u}_i$ to be scattered in the direction $\mathbf{u}$. Single and multiple scattering are separated here and are respectively expressed by the second and third terms on the right-hand side of Eq. (1).

In order to solve this equation, the angle variables θ and ϕ must be separated. Therefore, the scatterers being spherical, their phase function depends only on $\cos\gamma = \mathbf{u}\cdot\mathbf{u}_1$ and is expanded in ($\nu_{max}+1$) Legendre polynomials, calling on the associated Legendre polynomials P_l^m, where ν_{max} is determinated with the Wiscombe criteria [13]. With the same aim, the diffuse flux $f(\mu,\phi,\tau)$ is expanded in a Fourier series. One RTE is obtained for each component $f^{(m)}(\mu,\tau)$ of the Fourier series and reads as

$$\frac{df^{(m)}(\mu,\tau)}{d\tau} = -\frac{f^{(m)}(\mu,\tau)}{\mu} + \sum_{l=m}^{\nu_{max}} r_l^{(m)}(\tau)P_l^m(\mu)\left[\frac{F(\tau)P_l^m(\mu')}{\pi\eta_m|\mu'|}\right.$$
$$\left. + \int_{-1}^{1}\frac{f^{(m)}(\mu_1,\tau)}{|\mu_1|}P_l^m(\mu_1)d\mu_1\right], \quad (2)$$

with $r_l^{(m)}(\tau) = \varpi\alpha(l,m)\eta_m p_l(\tau)/4$, $\alpha(l,m)\eta_m = 2$ for $m=0$ and $\alpha(l,m)\eta_m = 2(l-m)!/(l+m)!$ for $m \neq 0$. Here $p_l(\tau)$ are the coefficients of the Legendre polynomials obtained by Mie theory for each kind of scatterer. These ($\nu_{max}-m+1$) integro-differential equations are coupled because of the multiple-scattering term and are ill conditioned for $\theta = \pi/2$ ($\mu=0$).

The AFM enables us to uncouple these equations, to transform them into integral equations, and to eliminate the ill conditioning. The auxiliary function $A_l^{(m)}(\tau)$ is introduced:

$$A_l^{(m)}(\tau) = \int_{-1}^{1}\frac{f^{(m)}(\mu_1,\tau)}{|\mu_1|}P_l^m(\mu_1)d\mu_1. \quad (3)$$

This quantity is introduced in Eq. (2) and leads [12] to the integral Fredholm equation (4) dealing with $A_l^{(m)}(\tau)$, which is easily solved:

$$A_l^{(m)}(\tau) = \sum_{l_1=m}^{\nu_{max}}\int_0^{\tau_h}[H^{(m)}(l,l_1,\tau,y) + U^{(m)}(l,l_1,\tau,y)](A_{l_1}^{(m)}(y)$$
$$+ s_{l_1}^{(m)}(y))dy. \quad (4)$$

The term $H^{(m)}(l,l_1,\tau,y)$ corresponds to the multiple scattering and is a function of the medium involving its albedo and its phase function. The term $U^{(m)}(l,l_1,\tau,y)$ depends on the boundary conditions, and at this step each case leads to its own expression. Finally, $s_l^{(m)}(y)$ is the source function of the radiative transfer equation due to the single scattering. In our case, where the incident light is collimated, it is written as

$$s_l^{(m)}(\tau) = F_k(\tau)P_l^m(\mu_k)/(\pi\eta_m|\mu_k|). \qquad (5)$$

The expressions for $H^{(m)}(l,l_1,\tau,y)$ and $U^{(m)}(l,l_1,\tau,y)$ applied to our particular case are given in Appendix A.

For each of the $(\nu_{max}+1)$ values of m, there are $(\nu_{max}-m+1)$ uncoupled integral equations (4) to be solved that are divergence free. This number of equations is equal to the number of unknown quantities $A_l^{(m)}$. Therefore the final system of integral equations is exact and does not need any assumption to be solved, which is not the case in the methods where an angular discretization is performed (N-flux and discrete ordinate methods) and an infinite values of directions and an infinite number of integro-differential equations would be necessary to describe the exact system. The auxiliary functions $A_l^{(m)}$ are numerically calculated. The $(\nu_{max}+1)$ components $f^{(m)}$ are then deduced and summed to obtain the diffuse flux f in each direction and for each wavelength. The global diffuse flux is deduced by integration over the upper half space. The reflectance factor, needed to compare the modeling with spectroscopic measurements, is then the sum of the integrated diffuse flux and the collimated flux calculated separately, if the upper surface is assumed to be a perfect diffuser. Finally, the reflectance factor for each wavelength of the visible spectrum are gathered to obtain the reflectance spectrum.

3. OPTICAL PROPERTIES AND REFLECTANCE SPECTRA OF HUMAN SKIN

The description of the stratified model and the optical properties of the scatterers are necessary for solving the RTE. We recall here the data already published that will allow us to obtain the albedo, the optical thickness, and the phase function with its expansion in Legendre polynomials of each layer or scatterer. These quantities are used to deduce the coefficients $r_l^{(m)}$ and $P_l^{(m)}$ that appear in $H^{(m)}$ and $U^{(m)}$ of Eq. (4) and that allow us to get the solution. We also point out the different parameters that influence skin color, commonly found in the literature, in order to later study their influence in a quantitative way.

Human skin is a natural stratified medium presented in Fig. 2. It can be divided into three main layers [1]. The most superficial one is the epidermis, which can also be divided into five sublayers called the stratum corneum, the stratum lucidum, the stratum granulosum, the stratum spinosum, and finally the stratum germinativum, which is the deepest. The thickness of the epidermis varies with the location of the skin on the body from 30 to 100 μm. The intermediate layer is the dermis, which is divided into the papillary dermis and the reticular dermis separated by the horizontal plexus. Its thickness can reach several millimeters. The deepest layer of the skin is the hypodermis, which can measure up to several centimeters.

Each main layer has specific scatterers. In the epidermis, melanin is contained in rather spherical cells called melanosomes. These cells are created in the deepest sublayer, the stratum germinativum. The melanosomes are fragmented [5], and their radius shortens as they move up from the lower to the upper layer. The skin color de-
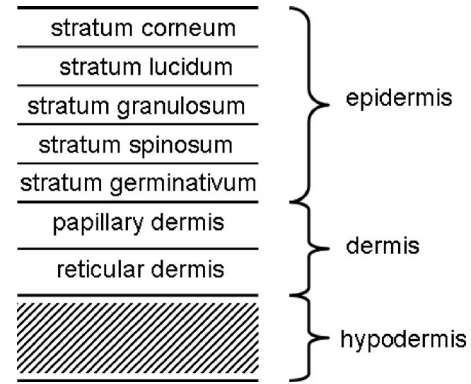

Fig. 2.   Skin structure.

pends on the volume concentration C of melanosomes contained in the epidermis. C can vary from 1% for lightly pigmented skins (Caucasian) to 46% for strongly pigmented skins (Negroid). Keratin is also contained in the epidermis and is located in cells called keratinocytes. In the dermis, there are veins containing red blood cells, composed of oxyhemoglobin HbO_2 and deoxyhemoglobin Hb. The skin color depends on the volume concentration CS of blood cells in the dermis and on the oxygen saturation S, which is the percentage of HbO_2 in the blood. In our model, the red blood cells are assumed to be spheres with the same volume as the real ones. CS varies from 1% to 10%. S varies from 30% for veins to 95% for arteries. The dermis is also constituted of collagen fibers, which have an effect on skin color. In the hypodermis, white fat and blood vessels are found.

A. Optical Properties of Scatterers

We first consider the melanosomes and the red blood cells that we assume to be spherical scatterers. We use Mie theory [8] in our own code to determine the absorption and scattering coefficients k and s of the scatterers that will allow us to express the albedo and optical depth and their phase function $p(\cos\gamma)$. The refractive index of the surrounding medium and the radius and complex refractive index of the scatterers are needed to implement Mie calculations. All these data are found in the literature, as specified afterward by a reference in each case. The embedding medium for each layer is assumed to have a refractive index equal to 1.36 [6].

Melanosomes. Melanosomes have a radius r ranging from 31.25 to 500 nm [6]. The complex refractive index of melanin is given by the following phenomenologic law according to Nielsen [6]:

$$\tilde{n}_{mel} = 1.57 + i\frac{\mu_a\lambda}{4\pi}, \qquad (6)$$

where λ is the wavelength in μm and μ_a is the absorption in μm^{-1}, whose variations are shown in Fig. 3. Mie calculations lead to the absorption coefficient k and the scattering coefficient s of the scatterers (Fig. 4). k and s decrease monotonically like μ_a when λ increases, and they increase with the radius. s dominates k except for the smallest melanosomes. The albedo ϖ and the optical depth τ can then be determinated. ϖ is independent of the volume concentration C and almost independent of the

wavelength in the visible range but increases with the radius from $\varpi = 0.4$ for $r = 31.25$ nm to $\varpi \approx 1$ for $r = 500$ nm. τ is proportional to C; it decreases with λ but increases with r and C. As shown in Fig. 5, the phase function $p(\cos \gamma)$ of the melanosomes depends on their radius. For the smallest scatterer ($r = 31.25$ nm), it tends to be isotropic, whereas for the largest scatterer ($r = 500$ nm), it presents a strong asymmetry with a predominantly forward scattering. The more anisotropic the phase function is, the larger the number of Legendre polynomials that are used in its expansion. For the smallest melanosomes, only four polynomials are needed. For the largest melanosomes, 22 polynomials are required. On the one hand, all these melanosomes are present in the studied medium. On the other hand, calculations are done simultaneously by taking into account the global system. The maximum order of the Legendre polynomials corresponding to the largest melanosomes must be taken into account in each slab, and the final runtime is proportional to this order. To reduce this runtime, we have studied the influence of this maximum order on the integrated diffuse flux and on the final reflectance factor. For more than eight polynomials,
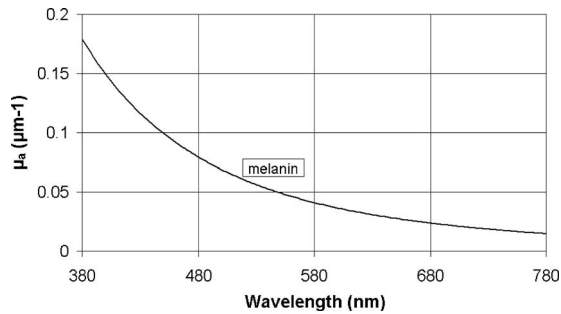

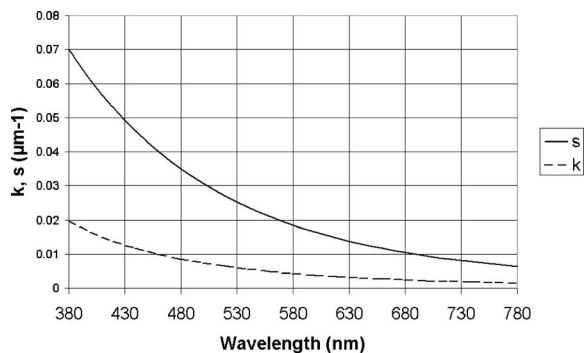Fig. 3. Variation of the absorption μ_a of melanin with λ.

Fig. 4. Variations of the absorption and scattering coefficients k and s with λ, for $r = 125$ nm.
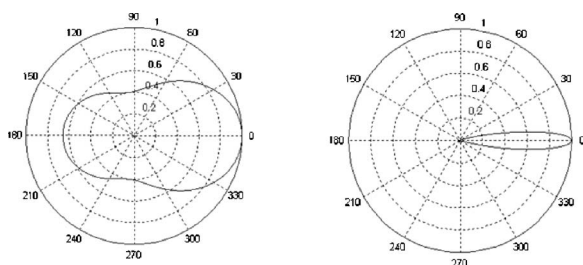

Fig. 5. Angular variation of the phase function at $\lambda = 380$ nm for two melanosomes $r = 31.25$ nm (left) and $r = 500$ nm (right).
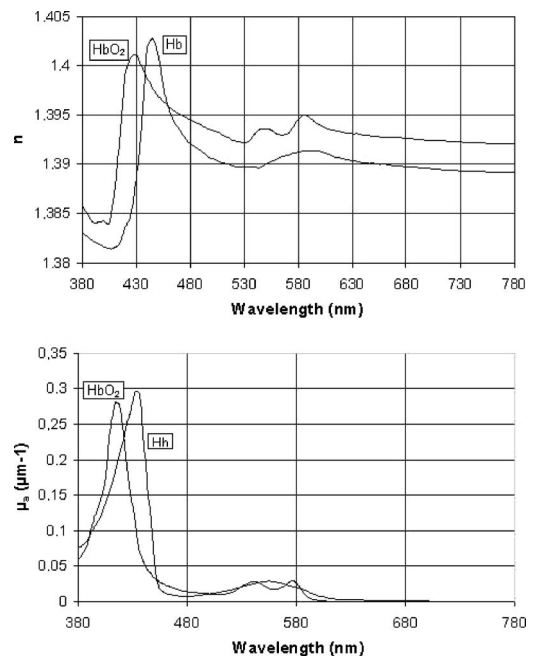

Fig. 6. Variations of the real parts of the refractive indexes (top) and of the absorption (bottom) of HbO_2 and Hb with λ.

the variation of the reflectance factor is always less than 1%, which is the experimental precision of the spectrometer. So we limit our expansion to the seventh order.

Red blood cells. Red blood cells are assumed to be spheres of 2.78 μm radius [14]. The refractive index of blood is taken as a linear combination of the refractive indexes of HbO_2 and Hb, so that $\tilde{n}_{blood} = n + i\kappa$, where $n = n_{HbO_2}S + n_{Hb}(1-S)$ and $\kappa = (\lambda/4\pi)[\mu_{a,HbO_2}S + \mu_{a,Hb}(1-S)]$. The variation of the real part of the refractive index [14] and of the absorption [15] μ_a of HbO_2 and Hb are shown in Fig. 6. Some wavelengths are noticeable, especially for $\mu_a(\lambda)$, where the minima will fit the maxima of the reflectance spectrum. Local minima for Hb at $\lambda = 480$ nm and for HbO_2 at $\lambda = 505$ nm and $\lambda = 560$ nm will thus be the signature of blood. Both absorptions are negligible for $\lambda \geq 600$ nm and will correspond to a large and rather constant reflectance factor in this range. The coefficients k and s of the red blood cells follow the combined absorption of HbO_2 and Hb, with s always larger than k. However, with our hypothesis red blood cells are large spheres with $r = 2.78$ μm, which implies an even more important forward scattering than the largest melanosomes. Mie calculations also give the asymmetric factor g, which is the proportion of light scattered forward, and here is larger than 0.99. Because of this strong anisotropy, 132 Legendre polynomials would be needed for the expansion of the phase function. That is why the blood scattering will be approximated below by the reduced scattering coefficient $s' = s(1-g)$ associated with an isotropic phase function. We then calculate the albedo and the optical depth of the red blood cells, and only the latter depends on the volume concentration CS of blood in the dermis. Figure 7 shows the variation of the albedo and of the optical depth of a blood cell according to λ for $CS = 2\%$ and $S = 30\%$ using k and s'.

Keratin and collagen. Unlike the previous scatterers, keratin and collagen fibers are not spherical. Even if it
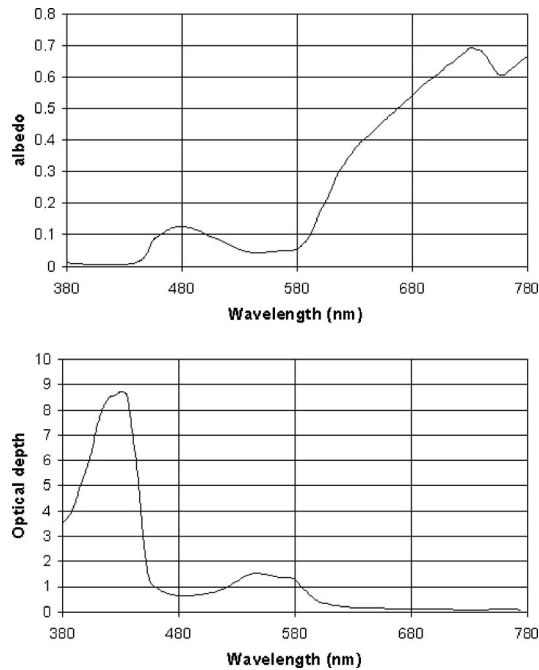
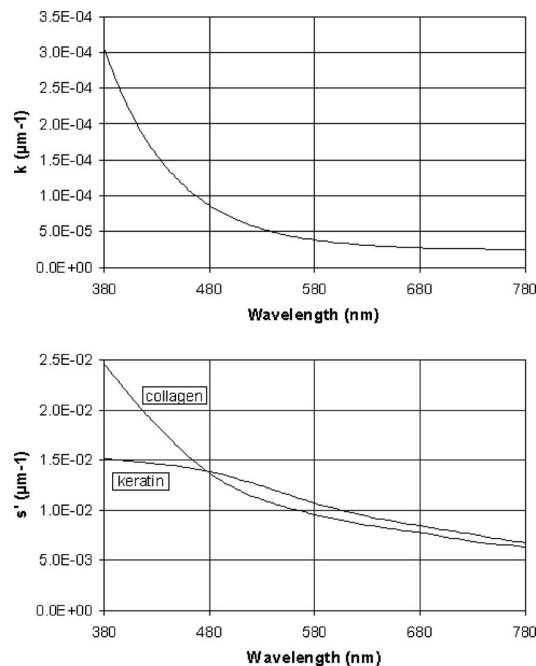Fig. 7. Variation of the albedo (top) and of the optical depth (bottom) for $CS=2\%$ and $S=30\%$ according to λ.

Fig. 8. Variation of the absorption coefficient k (top) and of the reduced scattering coefficients s' (bottom) of keratin and collagen fibers accordng to λ.

were possible to implement Mie calculations, the phase functions would not be expressed according to cos γ, and the AFM could not be applied. Consequently we use the absorption coefficients [16] k and the reduced scattering coefficients [17] s' found in the literature associated with an isotropic phase function as for blood. Their variations are presented in Fig. 8. Values of k are supposed to be identical [16] for keratin and collagen fibers, but s' values are different, mostly for small wavelengths. In the hypodermis, we will follow all the authors who do not care

about the absorption of blood vessels and consider only the scattering of white fat, which implies ϖ=1 associated with an isotropic phase function.

Every optical property of each layer is now determined by the couple (albedo, optical depth) and the phase function of the scatterers. They are introduced into Eq. (4), and the system is numerically solved at last to obtain the reflectance factor for each wavelength, as explained at the end of Section 2.

B. Skin Reflectance Spectra
To test the model, reflectance spectra of real skin were recorded to be compared with the modeling results. A class spectrophotometer CARY 5 is used, with an integrating sphere, which collects both the diffuse and specular light. The incident light is set at normal incidence. The reflected light is then collected in the same configuration as the results of our calculations. Typical reflectance spectra are presented in Fig. 9. It shows different measurements on real skin for two different subjects, at different locations and at different times separated by 14 days. We can notice in all these spectra that the wavelengths of the relative maxima are identical to the wavelengths of the absorption minima (λ between 460 and 505 nm and λ =560 nm).

The skin color depends on several factors, already quoted in the previous section and commonly used in the literature. First, the skin color varies according to the person, mainly because there are more or fewer melanosomes in the epidermis. Second, the color can be different on the same person according to the location on the body. Generally, different factors must be then taken into account:

- The volume concentration C of melanosomes,
- The volume concentration CS of blood in the dermis,
- The oxygen saturation S,
- The thickness of both epidermis and dermis.

Third, the outer conditions play a role in skin color. Measurements on the same person at the same place but separated by several days can show differences. In fact, the outside temperature and the hygrometry can change the structure of the skin, for example by modifying the thickness of the skin. Exposure to UV radiation can also change the skin color by increasing the number of melanosomes produced in the stratum germinativum and so changing the concentration of melanosomes C.
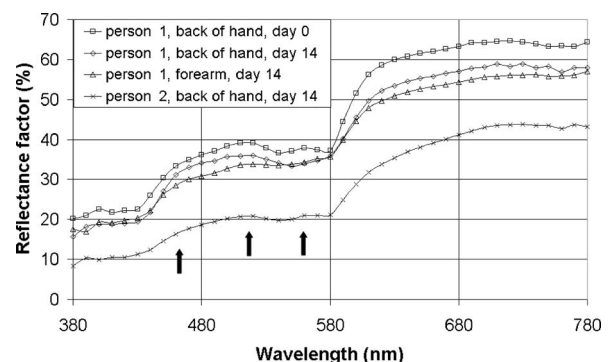

Fig. 9. Different reflectance spectra of real Caucasian skins.

4. MODELING RESULTS

A. From a 5-Layer Model to a 22-Layer Model

To study the reflectance spectra in the UV range, Nielsen *et al.* [6] proposed a model based on the skin stratification with 7 layers, presented in Fig. 10 (box 2). The epidermis is composed of five layers of equal thickness (10 μm) and equal volume concentration C of melanosomes. The radius of the scatterers embedded in the lower layer is 500 nm and is divided by two each time they move upward toward the upper layer. The dermis has a thickness of 2 mm and includes blood. Finally, the hypodermis of 3 cm thick skin does not absorb light as already mentioned. The calculations of Nielsen *et al.* [6] show that a strongly pigmented skin absorbs less UV radiation than a lightly pigmented skin owing to the scattering of melanosomes. They did not try to compare in detail the measured reflectance spectra with the modeling in the visible range. We try to do this, begining with their model.

In a first step, we consider the epidermis with the same five layers as Nielsen, containing only melanosomes in Figs. 10 (box 1). The light is assumed to be totally reflected at the lowest interface. Figure 11 shows the reflectance spectrum resulting from this model (squares) and its comparison with one of real skin (solid curve). Both spectra are different, except for their quasi-similar slope over 600 nm. The reflectance factor is too large, and all the characteristics, previously described and linked to the blood are obviously missing, showing that the blood is playing a great role in Caucasian skin color.

In a second step, we add the dermis and the hypodermis in a seven-layer model including red blood cells but without keratin and collagen fibers, Fig. 10 (box 2). The obtained reflectance spectrum is presented in Fig. 11 (diamonds) and is still not satisfactory. Although the characteristics due to the blood fortunately appear, the reflectance factor is too low for the short wavelengths and too large for wavelengths over 600 nm. This will be corrected by introducing the collagen fibers and the keratin, because they scatter more light in the short wavelengths.

In a third step, we add the keratin in the epidermis and the collagen fibers in the dermis. Unfortunately, for the epidermis melanosomes and keratin do not have the same phase functions, a mean phase function is not realistic, and the RTE is not currently adapted to such an inhomogeneous medium. Each of the five layers is then split into
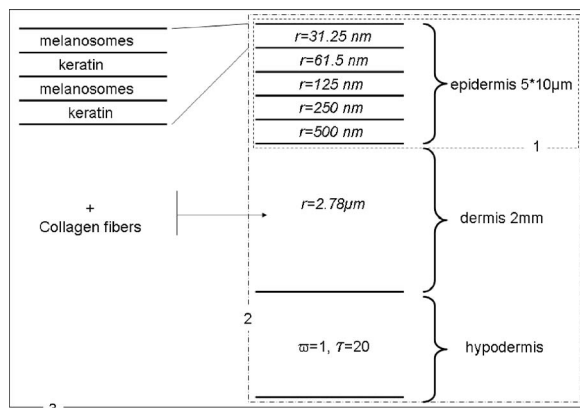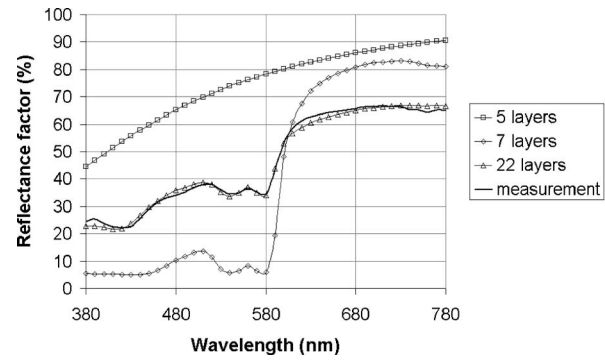

Fig. 11. Comparison between reflectance spectra for skin models of 5, 7, and 22 layers and a measured spectrum.

sublayers of the same thickness, containing only one type of scatterer. Several configurations with an increasing number of sublayers are tested, ensuring that the global optical thickness τ is equal to that of a unique layer 10 μm thick containing a mixture of both scatterers. The results are satisfactory for four sublayers, and over this number the reflectance factor does not vary more than our experimental precision. Each layer is then split into four parts, two sublayers containing melanosomes with the concentration C and two sublayers containing keratin with the concentration $(100-C)$. Moreover, the results are better when the upper sublayer contains melanosomes as shown in Fig. 10 (box 3).

For the dermis, the collagen and the red blood cells are assumed to have the same isotropic phase function, and it is not necessary to split the dermis into sublayers. The concentration of collagen fibers is assumed to be $(100-CS)$. Both scatterers can be considered to be contained in an homogeneous layer, with the scattering and the absorption coefficient being the sum of those of the red blood cells and of the collagen fibers with $s_{\text{dermis}}=s'_{\text{blood}}+s'_{\text{collagen}}$ and $k_{\text{dermis}}=k_{\text{blood}}+k_{\text{collagen}}$.

Our final satisfactory model is a 22-layer stratified medium, summarized in Fig. 10 (box 3). It leads to the spectrum presented in Fig. 11 (triangles) and is in excellent agreement with $C=1.5\%$, $CS=2\%$, $S=95\%$. In this case, the standard deviation ϵ between model and experiment is equal to 1.3%. It will be verified in the next subsection for different skins and thus for different values of the parameters.

B. Experimental Validation

The spectra for two different Caucasian persons at three different places (back of the hand, palm, and forearm) are represented as solid curves in Fig. 12. All of them have the same overall shape already discussed in the previous subsection. However, these spectra are different, with reflectance factors more or less large and with various slopes around 600 nm.

The spectra with symbols represent the results of the modeling after adjusting the parameters C, CS, and S and the total thickness of the epidermis to fit the experimental data. They are in rather good agreement with the measured spectra of real skin. Similar results were obtained with other persons. The same features due to the blood are present once more. However, it can be seen that the calculated spectra do not perfectly fit those of the real
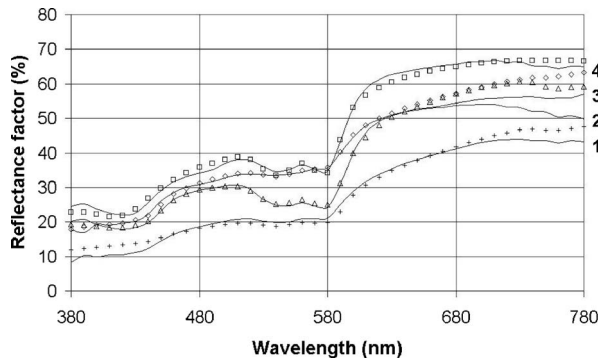

Fig. 10. Box 1, 5-layer model, box 2, 7-layer model, and box 3, 22-layer model.

Fig. 12.   Reflectance spectra of real skins (solid curves 1–4) and associated modeling (1, pluses; 2, triangles; 3, diamonds; 4, squares).

Table 1. Standard Deviation ϵ and Color Change ΔE Sets of Fig. 12

Set	ϵ	ΔE
1	2	4.4
2	4.6	2
3	2.8	0.8
4	1.3	2.7

skin for large wavelengths (red, over 630 nm). Nevertheless, this graphic difference has low impact on the final color change ΔE between experiment and modeling. This quantity is calculated from the coordinates L^*, a^*, and b^* of each spectrum (measured and modeled) in the CIE-Lab space (see Appendix B):

$$\Delta E = [(L^*_{\text{meas}} - L^*_{\text{mod}})^2 + (a^*_{\text{meas}} - a^*_{\text{mod}})^2 + (b^*_{\text{meas}} - b^*_{\text{mod}})^2]^{1/2}. \tag{7}$$

For a large reflectance factor, the relative gap is smaller. This conclusion can be seen in Table 1, where the standard deviation

$$\epsilon = \frac{\sqrt{\sum_N (R_{\text{meas}} - R_{\text{mod}})^2}}{N - 1}, \tag{8}$$

with $N=41$ being the number of wavelengths for which the modeling has been implemented between 380 and 780 nm, and the color change ΔE is calculated for each set of Fig. 12.

Actually, set 3 clearly shows that an important standard deviation due to the noticeable gap with a large reflectance factor for large wavelengths is associated with a small color change. The opposite case appears for set 1. After this validation, we are now able to fully use the possibilities of the modeling to go beyond experiments.

C. Influence of the Parameters
We here study the influence of the parameters already emphasized in previous sections: volume concentration C of melanosomes, oxygen saturation S, volume concentra-

tion CS of blood, and epidermal and dermal thicknesses. The reflectance spectra and the induced range of skin color change are calculated by changing only one of these parameters and are presented in Fig. 13.

First, the influence of the volume concentration C of melanosomes is shown in Fig. 13(a), for $S=50\%$, $CS=2\%$, and thicknesses of epidermis and dermis $z_e=50$ μm and $z_d=2000$ μm. As C varies from 1.5% to 7.5%, the reflectance spectrum is lowered and flattens; the features are smoothed. Actually, the number of melanosomes increases with C, and so does the light absorption. The less light reaches the dermis, the lower the scattered light by red blood cells and the smoother the features of the final spectrum. With this variation of C, the maximun skin color change ΔE is equal to 13.7.

Second, the influence of the oxygen saturation S is shown in Fig. 13(b), for $C=2\%$, $CS=2\%$, $z_e=50$ μm, and $z_d=2000$ μm. The reflectance factor of the plateau over 600 nm increases with S because HbO_2 absorption is smaller than that of Hb. This absorption also decreases more rapidly for HbO_2 than for Hb (Fig. 6), which explains the increase of the sharp slope in the spectra around 590 nm. The influence of HbO_2 can also be seen in the local maximum of the spectra at 560 nm: HbO_2 has a minimum of absorption at this wavelength that does not exist for Hb; therefore the reflectance factor increases with S. The last observation concerns the second local maxima of the spectra between 430 and 540 nm: its wavelength increases with S and is due to the different position of the local minimum of the absorption μ_a (Fig. 6, bottom) for HbO_2 and Hb. Finally, as S increases from 30% to 90%, the color change ΔE is equal to 3.6.

Third, the influence of the volume concentration CS of blood is shown on Fig. 13(c), for $C=2\%$, $S=50\%$, $z_e=50$ μm, and $z_d=2000$ μm. The reflectance spectra is lowered as CS increases. Moreover the spectrum flattens when CS decreases. The variation of the reflectance factor between 580 and 780 nm increases with CS. By looking at the mean absorption spectrum deduced from Fig. 6, the previous observation can be explained. As CS varies from 1% to 10%, the skin color change ΔE is equal to 13.5.

Fourth, the influence of the epidermal thickness z_e is shown in Fig. 13(d) for $C=1.5\%$, $S=70\%$, $CS=2\%$, and $z_d=2000$ μm. When the epidermis becomes thicker, the reflectance spectrum is lowered and flattens. As z_e varies from 50 to 70 μm, the skin color change ΔE is equal to 2.7.

Fifth, the influence of the dermal thickness z_d is shown in Fig. 13(e) for the same parameters and $z_e=50$ μm. In the same way, the reflectance spectrum is lower when z_d is larger but only in the plateau range, after 600 nm. As z_d varies from 1000 to 2000 μm, the skin color change ΔE is equal to 1.4.

On the one hand, these five parameters always influence the plateau, either on its reflectance factor or on its slope, and thus the redness of the skin. On the other hand, for smaller wavelengths, the influence of these five parameters on the spectra is variable: nil for z_d, low for S, a little more important for z_e, and important for CS and C. With the variation domains previously mentioned, the smallest color change is obtained by varying the dermal thickness, and the largest color change, as expected, is ob-
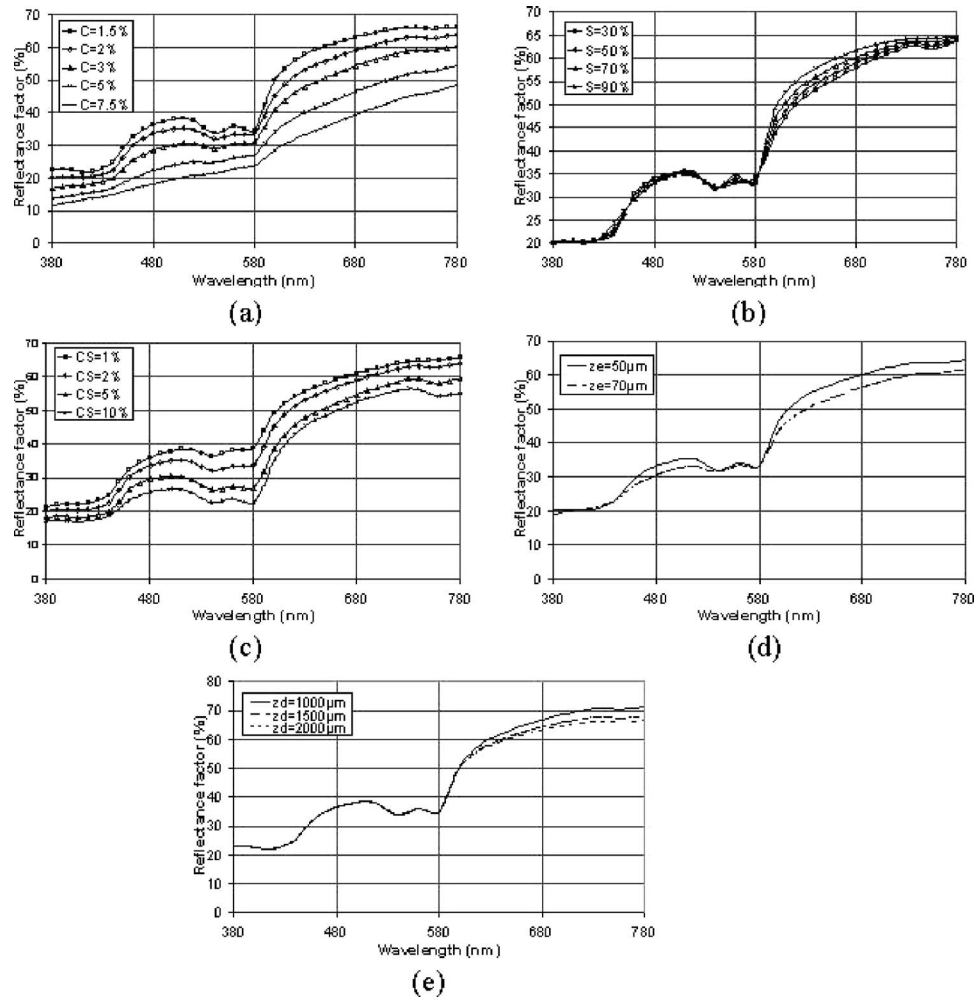
Fig. 13.   Influence of each parameter on the reflectance spectra: (a) volume concentration C of melanosomes, (b) oxygen saturation S, (c) volume concentration CS of blood, (d) epidermal thickness z_e, (e) dermal thickness z_d.

tained by varying the volume concentration C of melanosomes, which is the accurate parameter that discriminates Caucasian or Negroid skin types, for example.

5. CONCLUSION

This is the first time to our knowledge that RTE resolved by AFM has been applied to concrete examples and thus has been verified by experimental results. Starting from previous publications, a 22-layer model of human Caucasian skin has been developed and fully validated. Using this model, the results are satisfactory compared with the reflectance spectra of real skin by adjusting the characteristic parameters of the different scatterers as well as the different thicknesses of the layers. The possibilities of the model are then fully used for studying the influence of the characteristic parameters on the reflectance spectra of the skin and the corresponding color change, such as the volume concentration of melanosomes in the epidermis, the volume concentration and the oxygen saturation of blood in the dermis, the thicknesses of the epidermis and the dermis. Each of these parameters has a particular effect on the spectra and can be singled out. For Caucasian skin, although red blood cells lie under a 50 μm thick scattering medium, the influence of blood is predominant

in skin color and is emphasized in each feature of the spectra. The volume concentration of melanosomes generates an important variation of the spectra and thus of the skin color and explains the different colors according to ethnic pigmentation, localizations on the body, and tanning.

The successful stratified model and software developed in this study will be applied, in the near future, to model the color of Negroid and Asian skins, where the main differences with Caucasian skins are the size, the shape, and the space distributions of the melanosomes in the epidermis. The calculations will also be done for different configurations, bidirectional and backscattering ones. This last original configuration is fully justified because such a portable goniospectrophotometer is at our disposal and allows us to measure real skin reflectance spectra on any part of a body. A method allowing two scatterers with different phase function in the same layer will be developed. In this study, the interfaces have been assumed to be planar, so their roughness will be introduced later in the modeling. We already know that the rms roughness of the surfaces is larger than the wavelengths in the visible range, and this surface scattering, inducing an upward translation of the previous reflectance spectra, will not change their shapes. Finally, the effects of external condi-

tions, such as UV radiation, temperature, and hygrometry, will be analyzed and included in the model.

APPENDIX A: CALCULATIONS OF $A_l^{(m)}(\tau)$

The equation we have to solve is

$$A_l^{(m)}(\tau) = \sum_{l_1=m}^{\nu_{\max}} \int_0^{\tau_h} [H^{(m)}(l,l_1,\tau,y) + U^{(m)}(l,l_1,\tau,y)]$$

$$\times [A_{l_1}^{(m)}(y) + s_{l_1}^{(m)}(y)]\mathrm{d}y. \tag{A1}$$

We shall now express each term, $H^{(m)}(l,l_1,\tau,y)$ and $U^{(m)} \times (l,l_1,\tau,y)$, by taking into account the characteristics of our application. We consider a slab (1) with an optical thickness τ_h between an upper (0) and a lower (2) medium with refractive indices respectively named n_1, n_0, and n_2.

The boundary conditions for the diffuse flux are written, at each interface,

$$\text{for } \tau = 0, \qquad f^{+(m)}(\mu,0) = R_{10}f^{-(m)}(\mu,0), \tag{A2}$$

$$\text{for } \tau = \tau_h, \qquad f^{-(m)}(\mu,\tau_h) = R_{12}f^{+(m)}(\mu,\tau_h), \tag{A3}$$

where $f^{+(m)}$ and $f^{-(m)}$ are the diffuse flux, respectively, in the direction of increasing τ and decreasing τ and $R_{ij}(\mu)$ are the Fresnel's reflexion coefficients from medium i to medium j.

We are looking for the total flux, integrated on the upper half-space. Only the case $m = 0$ leads to a nonnull result, due to the integration on ϕ, and must be calculated.

The right-hand terms of Eq. (A1) are written as

$$H^{(0)}(l,l_1,\tau,y) = Cr_{l_1}^{(0)}(y) \int_0^1 \frac{P_l^0(\mu)P_{l_1}^0(\mu)}{\mu} \exp(-x/\mu)\mathrm{d}\mu, \tag{A4}$$

with $C = 1$ for $y < \tau$ and $C = (-1)^{l+l_1}$ for $y > \tau$,

$$U^{(0)}(l,l_1,\tau,y) = r_{l_1}^{(0)}(y) \int_0^1 \mathrm{d}\mu$$

$$\times \frac{P_l^{(0)}(\mu)P_{l_1}^{(0)}(\mu)}{\mu} \frac{1}{\exp(2\tau/\mu) - R_{10}(\mu)R_{12}(\mu)}$$

$$\times \left\{ R_{10}(\mu)R_{12}(\mu)\left[\exp\left(\frac{y-\tau}{\mu}\right) \right.\right.$$

$$\left. + (-1)^{l+l_1} \exp\left(-\frac{y-\tau}{\mu}\right) \right]$$

$$+ (-1)^l R_{12}(\mu)\exp\left(\frac{y+\tau}{\mu}\right)$$

$$\left. + (-1)^{l_1} R_{10}(\mu)\exp\left(-\frac{y+\tau}{\mu}\right)\exp\left(\frac{2\tau}{\mu}\right) \right\}. \tag{A5}$$

APPENDIX B: CIE-LAB SPACE

For more details concerning colorimetric caculations, see [18].

The trichromatic coordinates of the color are computed from the measured reflectance spectrum. These coordinates take into account the spectral density of the illuminant (λ), the three relative sensibility curves of the standard observer $\bar{x}(\lambda)$, $\bar{y}(\lambda)$, $\bar{z}(\lambda)$, and the diffuse reflectance spectrum of the sample (λ). Here the illuminant D65, which simulates daylight, and the standard observer defined by the CIE-1931 are chosen. The calculation of the X, Y, Z trichromatic components is first implemented according to

$$X = K \int S(\lambda)\bar{x}(\lambda)R(\lambda)\mathrm{d}\lambda,$$

$$Y = K \int S(\lambda)\bar{y}(\lambda)R(\lambda)\mathrm{d}\lambda,$$

$$Z = K \int S(\lambda)\bar{z}(\lambda)R(\lambda)\mathrm{d}\lambda,$$

$$K = \frac{100}{\int S(\lambda)\bar{y}(\lambda)\mathrm{d}\lambda}.$$

Then the $L^*a^*b^*$ space, defined by the CIE-1976, which is more uniform than the X, Y, Z space, can be deduced from the former according to

$$L^* = f\left(\frac{Y}{Y_B}\right),$$

$$a^* = \frac{500}{116}\left[f\left(\frac{X}{X_B}\right) - f\left(\frac{Y}{Y_B}\right) \right],$$

$$b^* = \frac{200}{116}\left[f\left(\frac{Y}{Y_B}\right) - f\left(\frac{Z}{Z_B}\right) \right],$$

with

$$f(A) = 116A^{1/3} - 16 \quad \text{if } f(A) \geq 8,$$

$$f(A) = \left(\frac{29}{3}\right)^3 A \quad \text{if } f(A)$$

$$\leq 8 \text{ (Pauli correction)}.$$

X_B, Y_B, and Z_B are the white reference XYZ coordinates ($R_B = 1$ for all of the visible range) with the chosen illuminant and standard observer.

The three coordinates of the CIE-Lab space are the achromatic lightness L^* and the two chromatic components: a^* (green–red axis) and b^* for the Cartesian coordinates.

REFERENCES

1. L. A. Goldsmith, *Physiology, Biochemistry, and Molecular Biology of the Skin* (Oxford U. Press, 1998).
2. S. Chandrasekhar, *Radiative Transfer* (Dover, 1960).
3. G. Poirier, "Human skin modelling and rendering," Master of Mathematics in Computer Science thesis (University of Waterloo, 2004).
4. P. Kubelka and F. Munk, "Ein Beitrag zur Optik der Farbanstriche," Z. Tech. Phys. (Leipzig) **12**, 593–601 (1931).
5. R. R. Anderson and J. A. Parrish, "Optical properties of human skin," in *The Science of Photomedicine* (Plenum, 1982), pp. 147–194.
6. K. P. Nielsen, L. Zhao, P. Juzenas, J. J. Stamnes, K. Stamnes, and J. Moan, "Reflectance spectra of pigmented and nonpigmented skin in the UV spectral region," Photochem. Photobiol. **80**, 450–455 (2004).
7. K. Stamnes, S. Chee Tsay, W. Wiscombe, and K. Jayaweera, "Numerically stable algorithm for discrete-ordinate-method radiative transfer in multiple scattering and emitting layer media," Appl. Opt. **27**, 2502–2510 (1988).
8. C. F. Bohren and D. R. Hoffman, *Absorption and Scattering of Light by Small Particles* (Wiley-VCH, 1983).
9. P. S. Mudgett and L. W. Richards, "Multiple scattering calculations for technology," Appl. Opt. **10**, 1495–1502 (1971).
10. M. Elias and G. Elias, "New and fast calculation for incoherent multiple scattering," J. Opt. Soc. Am. A **19**, 894–901 (2002).
11. L. Simonot and M. Elias, "Special visual effect of art glazes explained by the radiative transfer equation," Appl. Opt. **43**, 2580–2587 (2004).
12. M. Elias and G. Elias, "Radiative transfer in inhomogeneous stratified scattering media with use of the auxiliary function method," J. Opt. Soc. Am. A **21**, 580–589 (2004).
13. W. J. Wiscombe, "Improved Mie scattering algorithms," Appl. Opt. **19**, 1505–1509 (1980).
14. D. J. Faber, M. C. G. Aalders, E. G. Mik, B. A. Hooper, M. J. C. van Gemert, and T. G. van Leeuwen, "Oxygen saturation-dependent absorption and scattering of blood," Phys. Rev. Lett. **93**, 028102 (2004).
15. S. L. Jacques, http://omlc.ogi.edu/spectra/hemoglobin/index.html (1999).
16. S. L. Jacques, http://omlc.ogi.edu/news/jan98/skinoptics.html (1998).
17. M. J. C. van Gemert, S. L. Jacques, H. J. C. M. Sterenborg, and W. M. Star, "Skin optics," IEEE Trans. Biomed. Eng. **36**, 1146–1154 (1989).
18. G. Wyszecki and W. S. Stiles, *Color Science: Concepts and Methods, Quantitative Data and Formulae*, 2nd ed. (Wiley Interscience, 1982).